Journal of Pharmaceutical Analysis 14 (2024) 100926

Contents lists available at ScienceDirect

Journal of Pharmaceutical Analysis

journal homepage: www.elsevier.com/locate/jpa

Original article

Secondary metabolites of mulberry leaves exert anti-lung cancer activity through regulating the PD-L1/PD-1 signaling pathway

Guiqin Ye [a, b, c, 1], Xin Sun [a, 1], Jiuzhou Li [d], Yuanyuan Mai [c], Ruilan Gao [e, **], Jianbin Zhang [a, *]

[a] Cancer Center, Department of Medical Oncology, Key Laboratory of Tumor Molecular Diagnosisand Individualized Medicine of Zhejiang Province, Zhejiang Provincial People's Hospital, Affiliated People's Hospital, Hangzhou Medical College, Hangzhou, 310014, China
[b] Clinical Laboratory, Yuhuan City Hospital, Taizhou, Zhejiang, 317600, China
[c] Hangzhou Medical College, Hangzhou, 311300, China
[d] Department of Neurosurgery, Binzhou People's Hospital, Binzhou, Shandong, 256600, China
[e] Institute of Hematology Research, The First Affiliated Hospital of Zhejiang Chinese Medical University, Hangzhou, 310060, China

ARTICLE INFO

Article history:
Received 20 October 2023
Received in revised form
15 December 2023
Accepted 19 December 2023
Available online 22 December 2023

Keywords:
Moracin N
Click chemistry
PD-L1
T cell
Lung cancer

ABSTRACT

Lung cancer ranks the top of malignancies that cause cancer-related deaths worldwide. The leaves of *Morus alba* L are traditional Chinese medicine widely applied in respiratory diseases. Our previous work has demonstrated the anti-lung cancer effect of secondary metabolites of mulberry leaf, but their mechanism of action has still not fully elucidated. We synthesized Moracin N (MAN)-Probe conjugated with alkyne to label lung cancer cells and identified protein targets by chemical proteomic analysis. MAN and its probe exerted similar growth-inhibitory effect on human lung cancer cells. Chemical proteomic results showed that MAN targeted the programmed death ligand 1 (PD-L1) checkpoint pathway and T cell receptor (TCR) signaling pathway, indicating its immune-regulatory function. Cell-free surface plasmon resonance (SPR) results showed the direct interaction of MAN with PD-L1 protein. Molecular docking analysis demonstrated that MAN bound to E158 residue of PD-L1 protein. MAN downregulated the expression levels of PD-L1 in a time- and dose-dependent manner and disrupted the PD-L1/programmed death 1 (PD-1) binding, including other secondary metabolites of mulberry leaves Guangsangon E (GSE) and Chalcomoracin (CMR). Human peripheral blood mononuclear cells (PBMCs) co-cultured with MAN-treated A549 cells, resulting in the increase of $CD8^+$ $GZMB^+$ T cells and the decrease of $CD8^+$ $PD\text{-}1^+$ T cells. It suggested that MAN exerts anti-cancer effect through blocking the PD-L1/PD-1 signaling. *In vivo*, MAN combined with anti-PD-1 antibody significantly inhibited lung cancer development and metastasis, indicating their synergistic effect. Taken together, secondary metabolites of mulberry leaves target the PD-L1/PD-1 signaling, enhance T cell-mediated immunity and inhibit the tumorigenesis of lung cancer. Their modulatory effect on tumor microenvironment makes them able to enhance the therapeutic efficacy of immune checkpoint inhibitors in lung cancer.

1. Introduction

Improved understanding of the immune regulation in cancer development has led to impressive advances in the field of cancer immunotherapy over the last decade. Cancer cells often escape immune surveillance by manipulating the expression of immune checkpoint molecules on cancer or matrix cells [1]. Programmed death ligand 1 (PD-L1) is a type I integral membrane glycoprotein that expressed at the surface of tumor cells [2,3]. PD-L1 acts as a T-cell inhibitory checkpoint molecule which can inactivate tumor-infiltrating immune cells that express cell surface programmed death 1 (PD-1) [4,5]. When PD-1 is bound by PD-L1, the cytotoxicity $CD8^+$ T cells differentiate into exhausted $CD8^+$ T cells and play the role of immunosuppressive functions, thus inhibiting the immune activation and effector response [6]. In addition, PD-L1 also acts as an oncogene by limiting tumor cell apoptosis [7]. PD-L1

* Corresponding author.
** Corresponding author.
E-mail addresses: 19843009@zcmu.edu.cn (R. Gao), zhangjianbin@hmc.edu.cn (J. Zhang).
[1] Both authors contributed equally to this work.

https://doi.org/10.1016/j.jpha.2023.12.016

expression in lung cancer is a hallmark of adaptive resistance and its expression is often used to predict the efficacy of immunotherapy [8]. Thus, blocking the PD-1/PD-L1 axis is recognized as the attractive target for cancer immunotherapy [9,10]. However, clinical benefits do not occur in all patients and anti-PD-1 or anti-PD-L1 treatment is effective for less than 20% of cancer patients. Thus, it seems very necessary to develop new approaches to improve the efficacy of immunotherapy in cancer. Recently, combination therapy has become increasingly popular in treating this cancer. PD-L1 is a T-cell inhibitory checkpoint molecule that suppresses antitumor immunity. Anti-PD-L1 antibodies have shown remarkable promise in treating tumors, but the patient response rate is low. Therefore, small-molecule checkpoint inhibitors blocking PD-L1 function are urgently needed.

Through the ages, the leaves of *Morus alba* L are often prescribed to moisten the lung and relieve cough as traditional Chinese medicine, and are widely applied in respiratory system disease. Our previous phytochemical investigations have shown that mulberry leaves contain a large number of biologically important secondary metabolites, including Moracin N (MAN) [11,12]. It exhibits various biological properties, such as cytotoxic, anti-oxidant, anti-inflammatory, anti-bacterial, anti-microbial, and anti-viral properties. MAN leads to mitochondrial dysfunction in lung cancer and exerts an anti-cancer effect by inducing mitophagy [13]. In addition, the immunomodulatory effects of MAN has also been revealed. It stimulated the production of NO and prostaglandin E2 (PGE2) as immune response parameters and promoted the macrophagic differentiation, resulting in the increase of phagocytosis activity and cytokines secretion [14]. It also has been verified to improve humoral immune response through IgG production, or alleviate immunosuppression through the integrated modulation of the gut microbiota [15,16]. Here, we boldly guess that the effect of MAN extract on boosting immune response could be applied in lung cancer immunotherapy.

Although there are a large number of studies on the extraction of traditional Chinese medicine mulberry leaves, most of them are inductive studies and lack the verification of specific pathways and functions [17,18]. Due to the lack of a comprehensive perspective, previous studies inevitably left gaps in the understanding of these compounds [19]. So far, there is no any study on the identification of their binding targets. Thus, identification of protein targets will be a critical step in elucidating cellular mechanisms of action and revealing their complex biological activities. Recently, chemical proteomic approaches have been widely applied to screen the target proteins of natural products [20], which can provide a more comprehensive array of protein targets of active small molecules in an unbiased manner. This compound-centric chemical proteomics consist of the classical drug affinity chromatography and subsequent high-resolution mass spectrometry (MS) and bioinformatic analysis [21,22]. Generally, a cell-permeable activity-based drug probe (natural products) with an azide or alkyne moiety is first designed and synthesized [23]. Through click chemistry, a fluorescent tag or a biotin tag is attached to the probe-modified drug targets for visualization or affinity purification followed by MS analysis [23]. Thus, this quantitative proteomic approach is easy to distinguish specific targets of natural products from non-specific binding proteins.

In this study, quantitative chemobiological methods were used in combination with activity-based MAN-Probe and biological orthogonal click chemical reactions for target pull-down and MS identification. Our study comprehensively and impartially revealed the protein targets of MAN in lung cancer. Subsequent molecular biology and immunological verification studies confirmed that MAN binds to PD-L1 protein of lung cancer and enhances the function of T cells through the PD-L1/PD-1 axis. It could be a novel anti-cancer mechanism of secondary metabolites of mulberry leaves and can exert a synergistic anti-tumor effect to improve the efficacy of immunotherapy in lung cancer.

2. Materials and methods

2.1. Antibodies and reagents

These antibodies were purchased from Proteintech (Wuhan, China): PD-L1 (Cat No. 66248-1-Ig), FLAG (Cat. No. 20543-1-AP), GAPDH (Cat. No. 60004-1-Ig), Ki67 (Cat. No. 27309-1-AP), and CD3 (Cat. No. 65133-1). Other antibodies included anti-FLAG®, M2 affinity gel (Cat. No. A2220, Sigma-Aldrich, St. Louis, MO, USA), Phospho-Tyrosine Mouse mAb (P-Tyr-100) (Cat. No. 9411; CST, Boston, MA, USA).

Recombinant human proteins are listed as follows: interferon (IFN)-γ (Cat. No. MB5954; Meilunbio, Dalian, China), interleukin-2 (IL-2) (Cat. No. 589102; BioLegend, San Diego, CA, USA), PD-L1 (Cat. No. 156-B7-100; Novus Biologicals, Littleton, CO, USA), and PD-1 (Cat. No. Z03370; GenScript, Nanjing, China). Reagents used in our research included: TAMRA-biotin-azide (Cat. No. 1048-1; Click Chemistry Tools, Scottsdale, AZ, USA), biotin-azide (Cat. No. 908807-17-0; Cayman, Ann Arbor, MI, USA), and BeyoMag™ streptavidin magnetic beads avidin beads (Cat. No. P2151; Beyotime, Shanghai, China). Secondary metabolites of mulberry leaf were isolated and purified by Prof. Jingkui Tian from the Key Laboratory of Biomedical Engineering at Zhejiang University (Hangzhou, China).

2.2. Plasmids construction

The pCMV-Flag-PD-L1 vector was purchased from WZ Biosciences Inc. Site mutation of PD-L1 (E158Q, K136R, Y32F) was performed using QuickMutation™ Site-Directed Mutagenesis Kit) (Cat. No. D0206S; Beyotime, Shanghai, China) accordingly to the manufacture's instruction.

2.3. Cell culture

Peripheral blood mononuclear cells (PBMCs) were separated from peripheral blood obtained from healthy people using a lymphocyte separation medium (P8610; Solarbio, Beijing, China). Freshly isolated PBMCs were suspended in RPMI 1640 medium (CGM112.05; Cellmax, Hangzhou, China) supplemented with 10% superior grade fetal bovine serum (FBS, E510008; Sangon Biotech, Shanghai, China) and 1× penicillin–streptomycin solution (C0222; Beyotime, Shanghai, China). H460, A549 and Lewis lung carcinoma cells were obtained from the Cell Bank of Chinese Academy of Sciences (Shanghai, China). All cell lines were maintained in Dulbecco's modified Eagle medium (DMEM, CGM101.05; Cellmax, Hangzhou, China) containing 10% superior grade FBS in a 5% CO_2 atmosphere at 37 °C.

2.4. Cell proliferation assay with carboxyfluorescein diacetate succinimidyl ester (CFSE) labeling

A total of 2×10^6 cancer cells were plated in 6-well plates. After overnight, cells were stained with 1 μM CFSE (HY-D0938; MCE, Shanghai, China) in 2 mL DMEM medium at 37 °C for 20 min. The medium was discarded and cancer cells were co-cultured with PBMCs for 24 h. Cell fluorescence was analyzed by flow cytometry with 488 nm excitation.

2.5. Cell viability assay

Cell viability was measured using the CCK8 Assay Kit. 3×10^3 cells were seeded in 96-well plates and allowed to attach

overnight in a 5% CO_2 incubator. The cells were then treated with MAN (45 μM). After indicated treatment, 10 μL CCK-8 (Cat. No. C0037; Beyotime, Shanghai, China) was added to each well and the cells were subsequently incubated at 37 °C for 1–4 h. Absorbance was measured at 450 nm using the microplate reader.

2.6. Lactate dehydrogenase (LDH) release assay

PBMCs were first activated by 100 ng/mL CD3 antibody and then co-cultured with cancer cells at 10:1 ratio for 12 h. Cytotoxicity assay was conducted using a LDH cytotoxicity detection kit (C0016; Beyotime, Shanghai, China) according to the supplier's recommendations. The absorbance at 490 nm was measured using Synergy H1 (BioTek, Winooski, VT, USA).

2.7. In situ fluorescence labeling

A549 cells were cultured in six-well plates until 80%–90% confluence. MAN-Probe (10 μM) in 2 mL of medium was added and cells were incubated at 37 °C for 24 h. After treatment, cells were digested, resuspended in 100 μL phosphate buffer saline (PBS) and subjected to sonication. Centrifugation at 13,200 rpm was applied to remove the insoluble fraction from cell lysates. Equal amounts of extracted proteins (100 μg) were then subjected to fluorescence labeling. The click reaction was conducted by adding TAMRA-biotin-azide (10 μM), tris(2-chloroethyl) phosphate (TCEP; 1 mM; 100× fresh stock in water), tris [(1-benzyl-1H-1,2,3-triazol-4-yl) methyl] amine (TBTA) (100 μM; 100× stock in dimethyl sulfoxide (DMSO)), and $CuSO_4$ (1 mM; 100× stock in water) into cell lysates, followed by 2 h-incubation at room temperature. The labeled proteins were then acetone-precipitated, air-dried and solubilized with 100 μL sodium dodecyl sulfate (SDS) loading buffer. 50 μL sample was separated with 12% gradient SDS-polyacrylamide gel electrophoresis (PAGE) gel. Typhoon 9410 laser scanner (GE Healthcare, Boston, MA, USA) was used to obtain the gel images.

2.8. Liquid chromatography tandem-mass spectrometry (LC-MS/MS) analysis

The LC–MS/MS analysis was as described previously [24]. Tryptic hydrolysis was performed using filter aided proteome preparation (FASP) method, and peptide desalting was performed with C_{18} cartridge. The peptide was lyophilized and redissolved with 40 μL 0.1% formic acid solution and quantified. Buffer solution A was 0.1% formic acid aqueous solution and buffer solution B was 0.1% formic acid acetonitrile aqueous solution (84% acetonitrile). The column was balanced with 95% solution A, and the samples were loaded from the automatic injector to the column (Thermo Scientific Acclaim PepMap100, 100 μm × 2 cm, nanoViper C_{18}; Thermo Scientific, Waltham, MA, USA). They were separated by column (Thermo scientific EASY column ,10 cm, ID75 μm, 3 μm, C_{18}-A2) at a flow rate of 300 nL/min and analyzed by Q-Exactive series mass spectrometer. The original data for mass spectrometry analysis were RAW files, and MaxQuant software (version 1.5.3.17) was used for database identification and quantitative analysis.

2.9. PD-1-binding assay

Cells were harvested by trypsin digestion and centrifuged at 1,500 rpm for 5 min. The pellet was resuspended and washed twice with PBS and then incubated with recombinant human PD-1 Fc chimera protein for 1 h. After incubation with FITC-conjugated anti-human antibody (A0556; Beyotime, Shanghai, China), cell fluorescence was examined by flow cytometry with 488 nm excitation.

2.10. Cell isolation from tumor tissue

Cell isolation was performed according to a previous procedure with some adaptations [25]. Briefly, after execution, mice tumors were excised and cut into small pieces (< 2 mm in diameter). Tumor tissues were then digested in dissociation solution (1 mg/mL collagenase type III (C8490; Solarbio, Beijing, China), 100 μg/mL DNase I (D7073; Beyotime, Shanghai, China), 2.5 μg/mL hyaluronidase (H8030; Solarbio, Beijing, China)) for 1 h on a 37 °C shaker. Next, cell culture medium containing 10% FBS was added to dilute the suspensions. Cell suspensions were passed through 70 μm cell strainers, centrifuged at 1600 rpm and the lower layer was collected. Subsequently, erythrocytes were lysed with red blood cell lysis buffer (C3702; Beyotime, Shanghai, China), washed and resuspended in PBS.

2.11. Flow cytometry analysis

Cells were stained with the following antibodies: phycoerythrin (PE)-PD-1 (12-9985-81; Invitrogen, Waltham, MA, USA), FITC-CD8a (553030; BD, Franklin Lakes, NJ, USA), APC-Cy7-CD45 (557659; BD), V450-CD3 (561389; BD), and PE-Cyanine7-GZMB (25-8898-82; Invitrogen). Anti-CD16/CD32(553141; BD) was used to block non-specific binding. The cell suspension was stained with fluorescent dye coupled with antibody at 4 °C for 20 min. For intracellular staining, cell suspension was first fixed, permeabilized and dyed at 4 °C for 1 h. Cells were examined using NovoCyte Advanteon (Agilent, Santa Clara, CA, USA) and analyzed using NovoExpress software (Agilent).

2.12. Western blot analysis

Cells were lysed in radioimmunoprecipitation assay (RIPA) buffer (1% Triton X-100, 100 mM Tris-HCl pH 8.8, 100 mM NaCl, and 0.5 mM ethylenediamine tetraacetic acid (EDTA)). After centrifugation, cell lysates were collected and protein concentration was measured by bicinchoninic acid reaction. Protein samples were separated with SDS-PAGE, transferred onto polyvinylidene difluoride (PVDF) membrane, and blocked with 5% non-fat milk. Membranes were probed with the corresponding primary and secondary antibodies, respectively. Immunoblots were visualized with ChemiDoc Imaging Systems (Peiqing, Shanghai, China).

2.13. Immunofluorescence

Cells were fixed with 4% paraformaldehyde and permeabilized with 0.1% Triton X-100. They were stained with indicated first antibody overnight at 4 °C and (Alexa Fluor 549)-conjugated secondary antibody for detection. Hoechst staining was used for nuclear. Confocal microscope (Leica TCS SP5, Leica, Wetzlar, Germany) was used to detect cell fluorescence.

2.14. Molecular docking

The protein PD-L1 structure was obtained from the RCSB PDB crystal structure database (https://www.rcsb.org/), and SiteMap was used to predict the optimal small-molecule binding sites. The small molecule MAN structure was downloaded from the PubChem database (https://pubchem.ncbi.nlm.nih.gov/), and its three-dimensional structure was generated using a chemical information package RDKit. The molecular docking of MAN to PD-L1 domain was performed using AutoDock 4.2. The predicted active site was set as the docking center. During the docking process, the center coordinates X, Y, and Z were 18.17, −15.81, and −58.40,

respectively. Genetic algorithm was used for conformation sampling and scoring, and the optimal conformation was selected according to docking scores.

2.15. Surface plasmon resonance (SPR) assay

The binding affinity of MAN with PD-L1 was determined using a Biacore T200 instrument (GE, Boston, MA, USA) with a CM7 sensor chip. Briefly, recombinant PD-L1 proteins were loaded to the sensors using the Amine Coupling Kit (BR100050; Cytiva, Boston, MA, USA). Concentration-gradient MAN samples were prepared in a running buffer (PBS containing 0.05% P20, and 5% DMSO). The sensor and sample plates were placed on the instrument, and MAN samples flowed over the target sensors. Five concentrations were injected successively at a flow rate of 30 mL/min for a 200 s association phase, following by an 80 s dissociation phase at 25 °C. The final graphs were obtained by subtracting blank sensor and blank samples in duplex. Data were analyzed using Biacore T200 software.

2.16. Immunoprecipitation (IP)

As described in the technical bulletin of BeyoMag™ streptavidin magnetic beads, equal amount of biotin-labeled protein sample was incubated with avidin beads at 4 °C overnight with gentle rotation. The beads were washed with lysis buffer and the precipitates were boiled with gel electrophoresis sample buffer and analyzed via ChemiDoc Imaging Systems.

2.17. Xenograft tumor experiment

Male C57BL/6 mice (6 weeks old, purchased from Shanghai SLAC Laboratory Animal Co., Ltd, Shanghai, China) were acclimated for one week and then subcutaneously injected with 2×10^6 Lewis cells in the flank. Once the tumors reached approximately 100–200 mm^3, animals were randomly divided into 4 groups: Control, MAN, anti-PD-1 Ab or anti-PD-1 Ab plus MAN. Mice were intraperitoneally (i.p.) injected with MAN (40 mg/kg) or anti-PD-1 Ab (10 mg/kg) or in combination every 3 days. Mice of control group were injected with an equal volume of PBS. Tumor size was determined by digital calipers (length and width) every 5 days, and tumor volume (mm^3) was estimated using the formula (length $\times$ $width^2$)/2. The survival rate of mice was also recorded. After 32 days, the mice were euthanized under deep anesthesia and tumors were immediately excised and weighed. Mice blood was immediately collected in a sodium citrate tube and centrifuged at 5,000 rpm for 10 min. Serum was stored at −80 °C for subsequent alanine transaminase (ALT) and aspartate aminotransferase (AST) analysis. In addition, 1×10^6 Lewis cells were injected through tail vein to establish the tumor model of lung metastasis. Mice were treated as described above and mice lung was excised after execution. Hematoxylin and eosin (H&E) staining of mice lung nodules were performed in different groups.

2.18. H&E and immunohistochemical (IHC) staining

Mice liver tissue, lung tissue and subcutaneous tumor tissue samples were embedded in paraffin and antigen retrieval was performed. Following the blockade of endogenous peroxidase activity, samples were incubated with the primary antibodies, including Ki67, CD8, PD-1, PD-L1 and GZMB, and the appropriate secondary antibodies and reacted with DAB detection reagents (G1212, Servicebio, Wuhan, China). H&E staining was used to indicate tumor cells and nuclei of tumor sections.

2.19. Statistical analysis

All data represented at least three independent experiments. All experimental data were expressed as mean ± standard error of mean (SEM). Statistical analyses were performed using GraphPad Pro Prism 8.0 (GraphPad, San Diego, CA, USA). Unpaired two-tailed Student *t*-test or one-way analysis of variance (ANOVA) followed by Bonferroni's multiple comparisons test was employed to analyze the difference between sets of data. $P < 0.05$ was considered significant.

3. Results

3.1. Synthesis of MAN-Probe and measurement of its cytotoxicity

To profile and identify the targets of secondary metabolites of mulberry leaves, we chose MAN as a representative drug. First, we designed and synthesized a chemically engineered MAN-Probe with a clickable alkyne tag attached (Fig. 1A). The MAN-Probe was a white powder with a relative molecular weight of 406.1638. The theoretical molecular weight of target molecule should be 406.1649, and there was an obvious peak at 406.1638 *m/z* in the mass spectrum (Fig. 1B). The error was (406.1649 − 406.1638)/406.1649 × 100% = 2.7 ppm, less than 5 ppm. Thus, the compound at this position was the target molecule. The proton nuclear magnetic resonance (^{1}H-NMR) spectrum was as follows: (400 MHz, Methanol-*d*4) δ 8.55 (s, 1H), 7.32 (s, 1H), 7.07 (s, 1H), 6.91 (s, 1H), 6.73 (d, J = 2.2 Hz, 2H), 6.23 (s, 1H), 5.38–5.33 (m, 1H), 4.61 (s, 2H), 4.08 (s, 2H), 3.47 (d, J = 7.1 Hz, 2H), 3.34 (s, 1H), 1.77 (d, J = 4.8 Hz, 6H). It could be also seen from the hydrogen spectrum that the baseline was flat and there were no obvious miscellaneous peaks. The resolution of hydrogen spectrum was 5%, thus the purity of target product was about 95% (Fig. 1C). To further confirm that MAN-Probe possessed similar biological activity as the parent compound, lung cancer cells A549 and H460 were treated with MAN or MAN-Probe for 24 h or 48 h, respectively. CCK-8 assay results showed that there was no significant difference between MAN and its probe (Fig. 1D), suggesting that the addition of clickable alkyne tag does not interfere with drug activity.

3.2. Fluorescence labeling of MAN targets in live cells

In order to visualize the natural cellular protein targets of MAN, we first designed the research protocol according to relevant literature reports. In the first step, we verified the fluorescence labeling with MAN-Probe using fluorescent marker TAMRA-azide (Fig. 2A). In the second step, we conducted the immunoprecipitation experiment with biotin-azide and streptavidin (Fig. 2B). The proteins directly bound by MAN-Probe were eluted for MS analysis. Following this workflow, live A549 cells were treated with MAN-Probe for 24 h before lysis. The lysates were then reacted with TAMRA-azide through click chemistry followed by SDS-PAGE and fluorescence scanning. The results showed that a satisfactory level of labeling can be achieved with 10 μM MAN-Probe, which was chosen for subsequent *in situ* gel-based fluorescence labeling and pull-down experiments (Fig. 2C). To clarify the MAN bound protein targets in A549 cells, MAN-Probe-treated cells were examined with confocal microscopy to visualize the cellular distribution of MAN targets. A549 cells were labeled with MAN-Probe, fixed by paraformaldehyde and permeabilized by Triton X-100, and then conjugated with TAMRA-azide by click chemistry. As shown, MAN-Probe-labeled cells showed high levels of fluorescence in the cell membrane, cytosol and nucleus, whereas no fluorescence signal was observed in cells treated with DMSO or MAN (Fig. 2D).

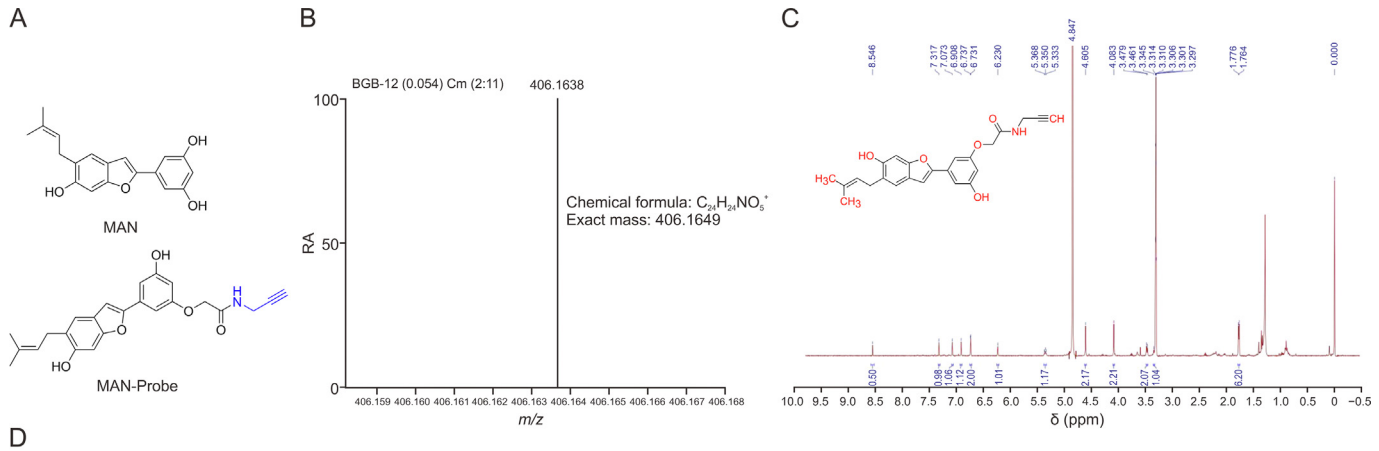

Fig. 1. Analysis of synthetic purity and cytotoxicity of Moracin N (MAN)-Probe. (A) The chemical structure of MAN and MAN-Probe. (B) Mass spectrometry analysis of MAN-Probe. Chemical formula: $C_{24}H_{24}NO_5^+$, exact mass: 406.1638. (C) Proton nuclear magnetic resonance (^{1}H-NMR) spectrum of MAN-Probe. (D) The cytotoxic effect of MAN and MAN-Probe on A549 and H460 cells. 10 μL CCK-8 solution was added into plate and the absorbance at 450 nm was measured.

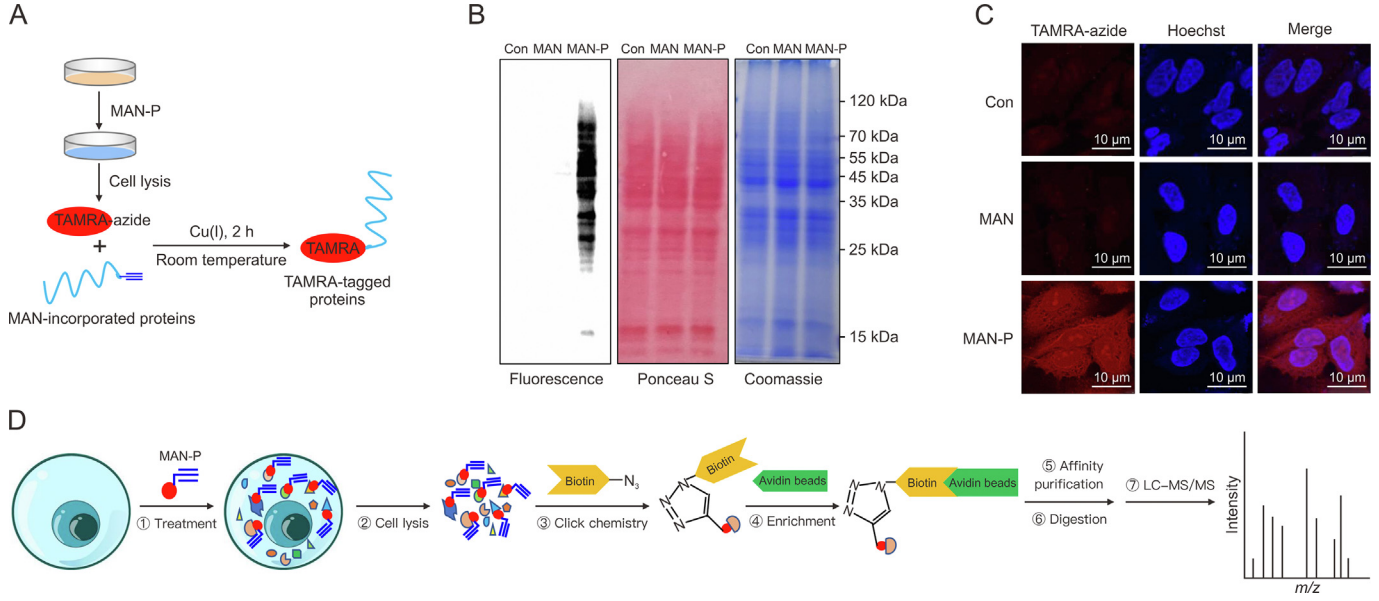

Fig. 2. Fluorescent labeling using Moracin N (MAN)-Probe in lung cancer cells. (A) Overall workflow for fluorescence *in situ* analysis of MAN potential targets in live cells. (B) General workflow for the chemical proteomics approach. Fluorescence labeling was used to study the activation mechanism of MAN, while biotin pulldown coupled with liquid chromatography tandem-mass spectrometry (LC-MS/MS) was used to identify the targets of MAN. (C) In-gel fluorescence analysis of A549 cells treated with MAN or MAN-Probe (10 μM). Ponceau S staining of membrane and Coomassie blue staining of western gel. (D) Confocal imaging of A549 cells treated with MAN or MAN-Probe (10 μM, 12 h). Cells were fixed and permeabilized for the click chemistry reaction. MAN-P: MAN-Probe; Con: Control.

3.3. Biological analysis of MAN targets by quantitative proteomics

Next, lLC-MS was used to identify the targets of MAN using MAN-Probe. In view of biological and experimental variations, two samples with or without MAN-Probe labeling were analyzed as biological replicates. Samples were first reacted with biotin-azide through click chemistry, followed by immunoprecipitation using magnetic streptavidin beads. MS was used to pool and analyze the derived peptides and finally the target proteins were identified and quantified. In our study, a total of 4,704 proteins were quantified by MS analysis. Among them, Venn diagram showed the overlapped protein targets and 837 differential proteins were chosen for further analysis (Fig. 3A and Table S1). Gene Ontology (GO) analysis results showed that many protein targets were localized in the nucleus, cytosol and mitochondrion (Fig. 3B). Biological process analysis revealed that a large number of differential proteins were involved

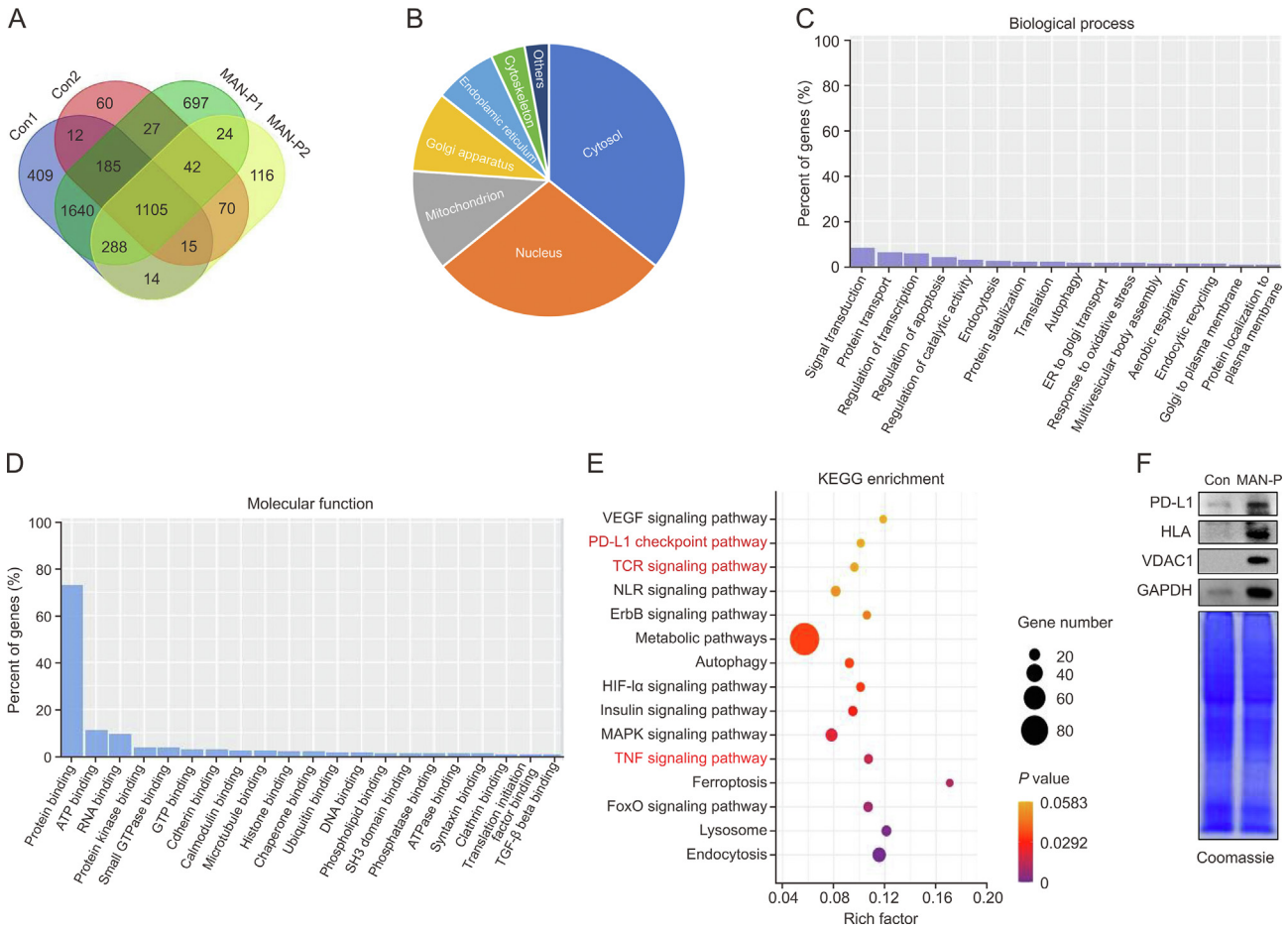

Fig. 3. Biological analysis of Moracin N (MAN) targets by quantitative proteomics. After MAN or MAN-Probe (10 μM) treatment, the protein samples of A549 cells after lysis were subjected to click reaction, and then the protein obtained after streptavidin beads co-immunoprecipitation (IP) was used for Coomassie staining. (A) Venn diagram showing the number of proteins identified using liquid chromatography-mass spectrometry (LC-MS) from A549 cells labeled with or without MAN-Probe. (B) Gene Ontology (GO) analysis of cellular localization of MAN targets. (C) GO analysis of the biological process of MAN targets. (D) GO analysis of the molecular function of MAN targets. (E) Kyoto Encyclopedia of Genes and Genomes (KEGG) enrichment scatter plot of MAN targets. (F) Western-blotting validation of the selected MAN-Probe targets. TCR: T cell receptor; TNF: tumor necrosis factor; VDAC1: voltage-dependent anion channel 1; GAPDH: glyceraldehyde-3-phosphate dehydrogenase.

in signal transduction, protein transport, protein stabilization, protein localization to plasma membrane, etc. (Fig. 3C). The molecular functions of the enriched proteins were associated with protein binding (ubiquitin, transforming growth factor-β (TGF-β), kinase, phosphotase, microtubule, chaperone, clathrin, and syntaxin), DNA binding, RNA binding, histone binding, phospholipid binding, etc. (Fig. 3D). Kyoto Encyclopedia of Genes and Genomes (KEGG) analysis showed that the enriched signaling pathways were mainly related with PD-L1 checkpoint, T cell receptor (TCR) signaling, tumor necrosis factor-alpha (TNF-α) signaling, etc. (Fig. 3E). To further verify that the identified proteins are direct binding targets for MAN, we performed pull-down experiments on representative proteins with MAN-Probe, followed by Western blotting with their respective antibodies (Fig. 3F). The results clearly confirmed the direct interaction between MAN-Probe and target proteins. These data suggest that MAN may change the expression of immune response-related molecules and signaling pathways in lung cancer, especially in the PD-L1/PD-1 signaling pathway.

3.4. MAN directly binds to PD-L1 protein

To confirm our findings, we used SPR to investigate the affinity between MAN and purified PD-L1 protein. The SPR assay results showed that MAN interacted with recombinant PD-L1 coated surface in a dose-dependent manner and the calculated affinity was $K_D = 5.48 \times 10^{-12}$ (M) (Fig. 4A). Based on these results, we constructed a proposed model for the reaction between MAN and PD-L1 (Fig. 4B). Since we failed to obtain a crystal structure of complex, we could only attempt to understand the interaction at the molecular level by simulating a molecular model using molecular docking. We used AutoDock4.2 software to conduct molecular docking experiments, set the predicted active site as the docking center, used genetic algorithm to conduct conformational sampling and scoring, and selected the optimal conformation according to the docking score [26]. The interaction between PD-L1 and small molecule MAN were mainly divided into hydrogen bonding, π-π stacking, hydrophobic interaction and polar van der Waals contact. One hydroxyl group on the benzene ring formed a hydrogen bond with the skeleton carbonyl group of Lys136; one hydroxyl group formed a hydrogen bond with the side chain carbonyl oxygen of Glu158; one hydroxyl group formed a hydrogen bond with the skeleton carbonyl group of Tyr32 (Fig. 4C). The π-π stacking was formed by the charge center of benzene ring of MAN and the charge center of side chain phenol of Tyr32. In addition, the hydrophobic skeleton of MAN interacted with the surrounding hydrophobic amino acids (Ile137, Pro133, Ala157). Some of the surrounding polar amino acids, such as Lys105, Gly33, and Asp103 (magenta), had van der Waals contact due to close contact.

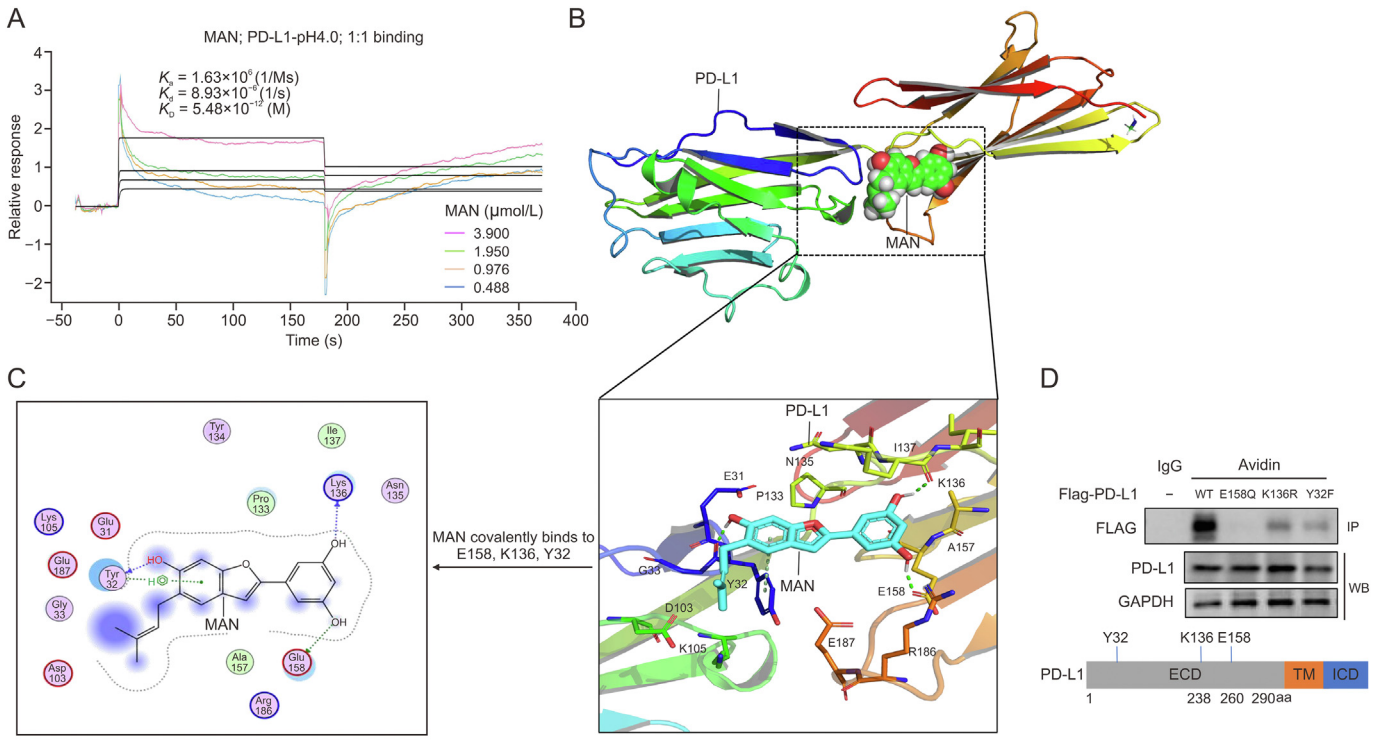

Fig. 4. Moracin N (MAN) directly targets programmed cell death 1 ligand 1 (PD-L1) protein. (A) Surface plasmon resonance (SPR) was performed to analyze the binding interaction of PD-L1 with different dosages of MAN and the evaluation of dissociation constant (KD) value was shown. (B, C) Molecular docking analysis of MAN covalently binding to PD-L1 protein. An overview of binding pattern of MAN with PD-L1 protein. (D) The detailed binding mode of MAN with PD-L1 protein. The reaction of MAN (sticks model) with different residues (E158, K136 and Y32) of PD-L1 protein (sticks and cartoon models, protein data bank (PDB) ID: 7ALV) was shown. Green dotted line: hydrogen bonding; O atom: red; N atom: blue; C atom: cyan. ECD: extracellular domain; TM: transmembrane domain; ICD: intracellular domain; WB: Western blotting; GAPDH: glyceraldehyde-3-phosphate dehydrogenase.

The above structure analysis revealed that MAN bound to the interface of PD-L1 domain. Next, key interactions like hydrogen bond with Glu158, Lys136 and Tyr32 residues of PD-L1 protein were further analyzed, because these three residues localized in the extracellular domain of PD-L1, which played a crucial role in their interaction. We did site-directed mutagenesis of PD-L1 and then examined the binding of MAN to PD-L1 protein. Interestingly, mutation of E158 resulted in the loss of MAN and PD-L1 interaction while mutations of K136 and Y32 only attenuated the binding of MAN to PD-L1 (Fig. 4D), indicating that MAN targets PD-L1 at E158 with the highest interaction affinity.

3.5. MAN serves as a PD-L1 regulator

Based on the above analysis, MAN targeted PD-L1 molecule of lung cancer cell. Cell viability analysis displayed that MAN had a better effect on inhibiting the proliferation level of tumor cells with high expression of PD-L1 compared with the control group (Fig. S1A). In order to further explore the role of MAN in regulating the PD-1/PD-L1 signaling pathway, we examined the effect of MAN on PD-L1 expression. As shown in Figs. 5A and B, Western blotting results showed that MAN treatment reduced the levels of PD-L1 in lung cancer cells A549 and H460 in a time- and dose-dependent manner while the level changes of human leukocyte antigen (HLA) was not significant. In addition, the mRNA levels of PD-L1 was also measured and MAN treatment resulted in its significant increase (Fig. S1B). Flow cytometry analysis and confocal imaging revealed that MAN significantly reduced the levels of cell surface PD-L1 in H460 and A549 cells, indicating MAN could also reduce the PD-L1 conveyed to cellular plasma membrane (Figs. 5C–F). As a tumor cell surface protein, PD-L1 can be upregulated in response to IFN-γ by activated T cells [27]. We next examined whether MAN also affects the expression level of inductive PD-L1. As shown, IFN-γ stimulated the expression level of PD-L1 in A549 and H460 cells, and MAN treatment significantly downregulated IFN-γ-induced PD-L1 expression (Figs. 5G and H), indicating its regulatory effect on T cells function. But the levels of HLA did not change too much under MAN treatment. Altogether, the above results demonstrated that MAN decreases both constitutive and inductive PD-L1 expression in lung cancer.

PD-L1 can be regulated by phosphorylation, which affects its stability, subcellular localization and function. It has been reported that glycogen synthetase kinase 3β (GSK3β) and AMP-activated protein kinase (AMPK) can phosphorylate PD-L1 protein at serine or threonine residues, thereby destroying the stability of PD-L1 and triggering the degradation of PD-L1 [2,28]. In addition, PD-L1 phosphorylation also occurs at tyrosine reside [29]. In response to MAN treatment, immunoprecipitation results showed the increase of PD-L1 phosphorylation level at tyrosine reside (Fig. 5I), which could be responsible for the decrease of PD-L1 protein stability.

3.6. GSE and CMR are also verified as a PD-L1 regulator

GSE and CMR are novel secondary metabolites isolated from mulberry leaves, a traditional Chinese medicine widely applied in respiratory diseases. Our previous study showed that GSE and CMR have cytotoxic effect on lung cancer [30,31]. Here, we also examined their regulatory effect on PD-L1 of lung cancer cells. Western blotting results showed that GSE treatment reduced the expression levels of PD-L1 in A549 and H460 cells in a time- and concentration-dependent manner (Figs. S2A and B). Similarly, CMR also exerted the inhibitory effect on PD-L1 expression of lung

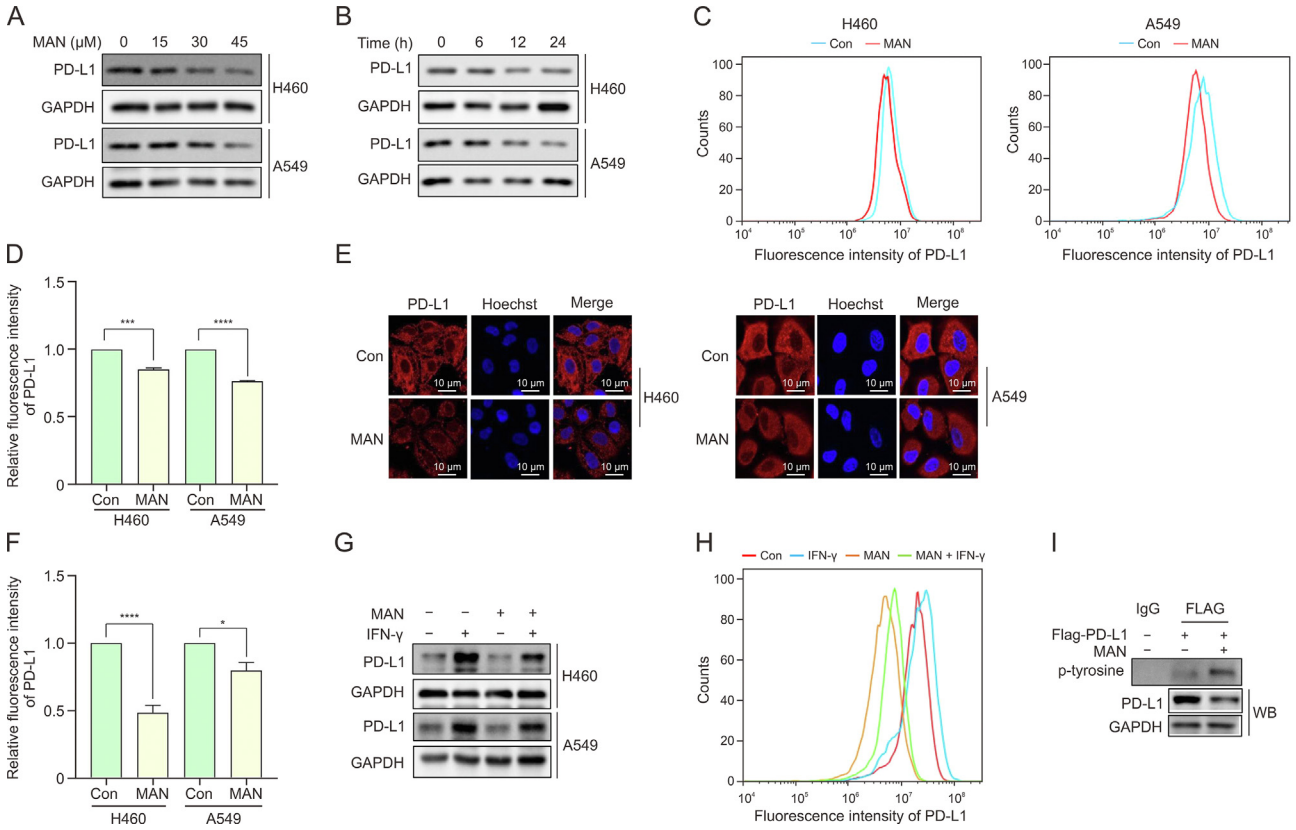

Fig. 5. Moracin N (MAN) serves as a programmed cell death 1 ligand 1 (PD-L1) regulator. (A, B) Western blotting analysis of PD-L1 and human leukocyte antigen (HLA) expression in H460 and A549 cells. Cells were treated with different concentrations of MAN for 24 h (A), or 30 μM MAN for the indicated time (B). (C, D) H460 and A549 cells were treated with MAN (30 μM, 24 h) (C) and the levels of PD-L1 was detected by flow cytometry(D). Statistical analysis of PD-L1 intensity was also shown. $^{***}P < 0.001$, $^{****}P < 0.0001$. (E, F) Confocal imaging of PD-L1 expression in lung cancer cells treated with MAN. Statistical analysis of PD-L1 intensity was shown. $^{*}P < 0.01$, $^{****}P < 0.0001$. (G, H) H460 and A549 cells were stimulated with interferon (IFN)-γ (5 ng/mL, 2 h) and then treated with MAN (30 μM, 24 h). The expression levels of PD-L1 and HLA were detected by Western blotting or flow cytometry, respectively. (I) HEK293 cells were transfected with Flag-PD-L1 and then treated with MAN. Cell lysates were applied to immunoprecipitation (IP) using anti-FLAG® M2 affinity gel and Western blotting (WB) was used to examine the levels of phospho-tyrosine. GAPDH: glyceraldehyde-3-phosphate dehydrogenase.

cancer cells (Figs. S2C and D). Confocal assay also revealed that GSE and CMR significantly reduced the cell surface PD-L1 in A549 cells, indicating the reduction of PD-L1 conveyed to plasma membrane (Figs. S2E–G). Finally, we examined whether the inductive PD-L1 expression could be influenced. As expected, GSE and CMR attenuated IFN-γ-induced PD-L1 expression in A549 cells (Figs. S2H–J). In conclusion, these results demonstrate that secondary metabolites extracted from mulberry leaves also downregulate PD-L1 expression in lung cancer cells.

3.7. MAN attenuates the interaction of PD-L1 and PD-1 and enhances $CD8^+$ T cell function in vitro

When PD-L1 binds to PD-1 on T cells, it induces inhibitory signal and shuts down the anti-tumor activity of T cells [32]. We next examined whether MAN treatment affected the binding of PD-L1 to PD-1. A cell imaging approach was used to re-create the interaction between PD-L1 and PD-1 *in vitro* [2]. A549 cells were incubated with recombinant human PD-1 Fc chimera protein and secondary antibody conjugated with Alexa Fluor 488 dye, respectively. The interaction between PD-L1 and PD-1 on cellular plasma membrane can be determined through cellular fluorescence. As shown, green fluorescence intensity was decreased in MAN-treated H460 and A549 cells, indicating the reduced binding of PD-L1 to PD-1 (Figs. 6A and B). Consistently, flow cytometry results also showed that MAN significantly reduced the green fluorescence intensity of H460 and A549 cells with increasing dose (Figs. 6C and D). The similar results were also shown in lung cancer cells in response to GSE and CMR treatment (Figs. S3A and B). Taken together, these results demonstrate that secondary metabolites from mulberry leaves attenuated the immunoinhibitory effect on T cells by disrupting the interaction of PD-L1 and PD-1.

3.8. Effect of MAN treatment on T cell function

To evaluate whether T cells activity could be changed, we co-cultured MAN-pretreated A549 cells with activated T cells and the cytotoxicity of T cells was determined. As shown, MAN pretreatment increased the proportion of $CD8^+$ IFN-γ^+ T cells (cytotoxic T cells) and decreased the proportion of $CD8^+$ PD-1^+ T cells (exhausted T cells) (Figs. 6E–G), indicating the enhanced cytotoxicity of T cells. Moreover, a dose-dependent manner was also shown in the enhancement of T cell function by MAN. But the proportion of $CD4^+$ T cells did not change too much (Fig. S4). The similar results were also shown in the co-culture of GSE-pretreated A549 cells and T cells (Fig. S3C). These results demonstrated that secondary metabolites from mulberry leaves can enhance T cell-mediated immunity through relieving the immunoinhibitory effect of PD-1 molecule.

Next, we determined the cytotoxicity of T cells on lung cancer cells. CFSE labeling assay results showed that activated T cells significantly killed a large number of A549 cells (Fig. 6H). Under MAN pretreatment, more cancer cells were killed by T cells, which was in accordance with the dose of MAN. LDH cytotoxicity assay results also showed that activated T cells significantly

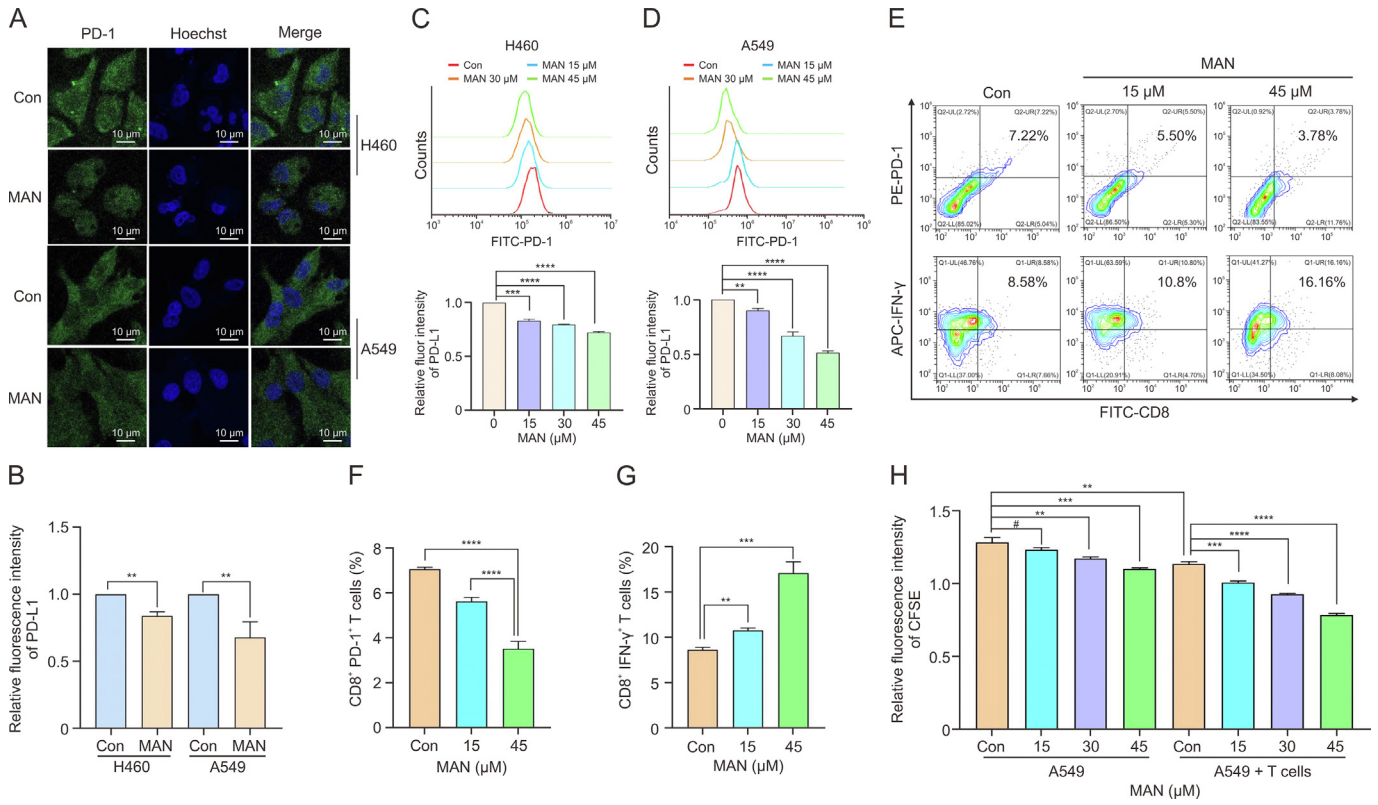

Fig. 6. Moracin N (MAN) attenuates the interaction of programmed cell death 1 ligand 1 (PD-L1) and programmed cell death 1 (PD-1) and enhances $CD8^+$ T cell function *in vitro*. (A) PD-L1/PD-1 binding assay in A549 or H460 cells. Cells were first treated with MAN (30 μM, 24 h) and then stained with recombinant human PD-1 protein. The nuclei were stained with Hoechst. (B) As in Fig. 6A, bound PD-1 was calculated and statistically analyzed according to cellular fluorescence intensity. $^{**}P < 0.01$. (C, D) H460 (C) and A549 (D) cells were treated with different concentrations of MAN for 24 h and then stained with recombinant human PD-1 protein. Bound PD-1 was detected by flow cytometry and statistically analyzed. $^{**}P < 0.01$, $^{***}P < 0.001$, $^{****}P < 0.0001$. (E) A549 cells were pre-treated with or without MAN (15 or 45 μM) for 6 h and then co-cultured with human peripheral blood mononuclear cells (PBMCs) for 24 h. After labeling with indicated antibodies, cell fluorescence was measured using flow cytometry. (F, G) As in Fig. 6E, the proportion of $CD8^+PD\text{-}1^+$ (F) or $CD8^+$ interferon (IFN)-γ^+ (G) T cells in human PBMCs were statistically analyzed. $^{**}P < 0.01$, $^{***}P < 0.001$, $^{****}P < 0.0001$. (H) A549 cells were first labeled with carboxyfluorescein diacetate succinimidyl ester (CFSE) and then pre-treated with different dosages of MAN for 6 h. They were co-cultured with human PBMCs for 24 h and flow cytometry was used to detect the fluorescence intensity of A549 cells. $^{\#}P > 0.05$, $^{*}P < 0.01$, $^{**}P < 0.01$, $^{***}P < 0.001$, $^{****}P < 0.0001$.

increased LDH release from A549 cells (Fig. S3D). In the pre-treatment of GSE, more LDH release from A549 cells were also detected by T cells, which was dose-dependent. The above results demonstrated that pretreatment with secondary metabolites from mulberry leaves enhances the cytotoxicity of T cells on lung cancer cells.

3.9. MAN suppresses lung tumor growth by modulating immune microenvironment

To determine whether MAN exerts anti-lung cancer activity *in vivo*, tumor xenograft model was constructed through subcutaneously injected Lewis cells into the flank of C57BL/6 mice. Tumor-bearing mice were i.p. administrated with MAN or anti-PD-1 antibody alone or together. As shown in Fig. 7A, administration of MAN or anti-PD-1 antibody significantly suppressed tumor growth and anti-tumor efficacy was further enhanced in the combination therapy group. The average tumors weight either in MAN- or anti-PD-1 antibody-treated group was significantly lighter than that of control group and mice of the combination therapy group had the smallest tumor size (Figs. 7B and S5A). In addition, we also examined the therapy efficacy of MAN on tumor lung metastasis. H&E staining of mice lung results showed that administration of MAN or anti-PD-1 antibody reduced the number of malignant lung nodules, and lung nodules were hardly detected in the mice of the combination therapy group (Fig. 7C).

During the treatment period, administration of MAN alone or together with anti-PD-1 antibody had no significant effect on mice body weight (Fig. S5B). To further evaluate the toxicity and side effect of drug treatment, we collected mice serum and liver of different treatment group and performed serum biochemistry analysis. The serum levels of ALT and AST were slightly increased under anti-PD-1 antibody treatment alone or together with MAN (Fig. S5C). H&E staining also showed no obvious liver pathological changes (vacuolation, hepatic sinusoid congestion and inflammatory infiltration) in mice treated with MAN alone or together with anti-PD-1 antibody (Fig. S5D). The above results demonstrated the safety of MAN treatment combination with anti-PD-1 antibody in lung cancer.

To confirm the role of MAN in anti-tumor immunity *in vivo*, we determined the expression levels of immunity-related molecules. At first, the levels of Ki67 (a marker of proliferation) were examined, and it was decreased in different treatment group and the combination treatment group had the least levels of Ki67 (Fig. 7D). Immunohistochemistry assay results showed that the levels of PD-L1were decreased either in MAN or anti-PD-1 antibody alone or combination treatment (Fig. 7D). Based on the literature, the decrease of exhausted T cells indicates a shift toward an activated immune microenvironment [33]. In tumor-infiltrating lymphocyte (TILs) profile analysis, the proportion of activated cytotoxic T cells (GZMB and CD8 double positive) were markedly increased with MAN or anti-PD-1 antibody treatment and it was increased the

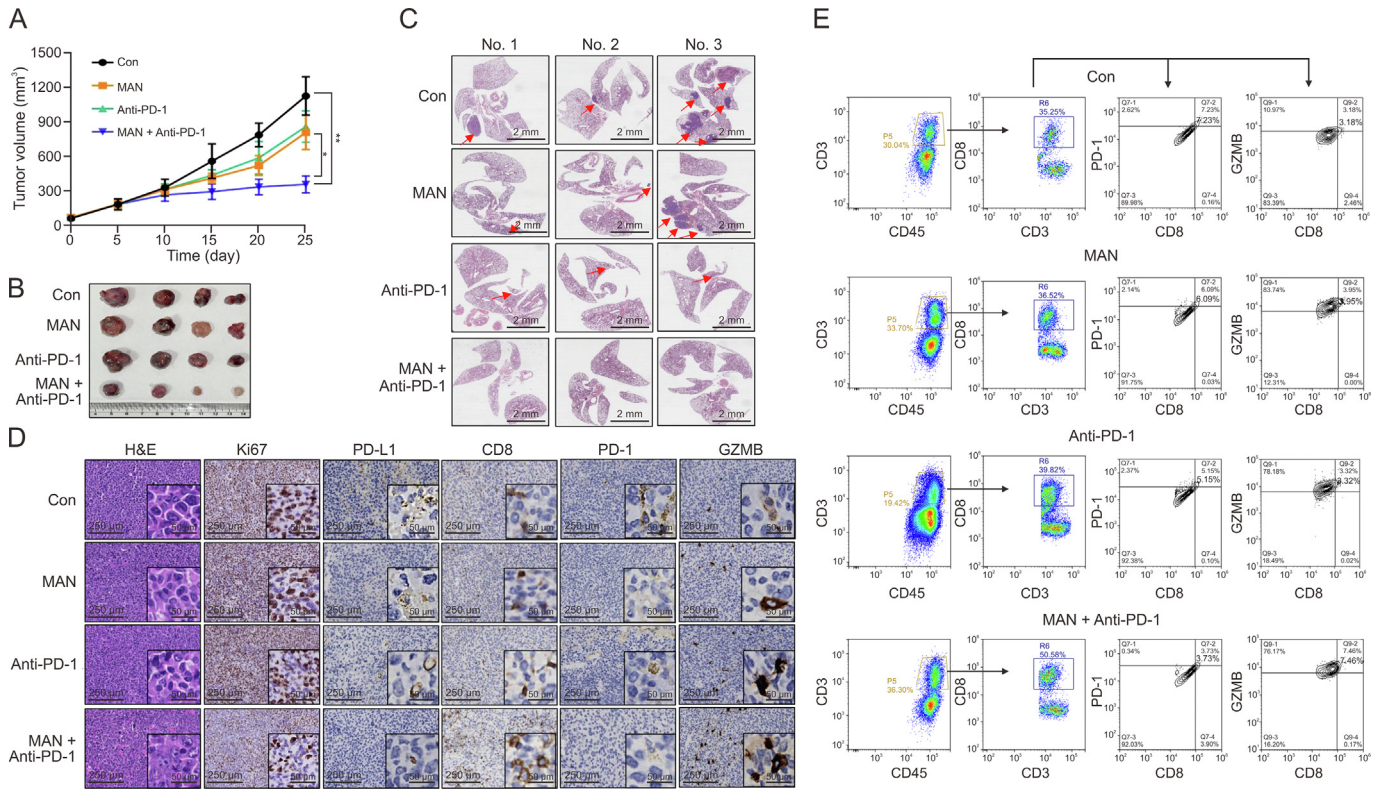

Fig. 7. Combination treatment of Moracin N (MAN) and anti-programmed cell death 1 (PD-1) effectively inhibits lung cancer growth *in vivo*. (A) Lewis cells were subcutaneously injected into the flank of C57BL/6 mice to establish the tumor model. Mice were intraperitoneal injected with MAN or anti-PD-1 antibody alone or together. Mice tumor volume of different groups was calculated and statistically analyzed. $^{*}P < 0.05$, $^{**}P < 0.01$. (B) After execution, mice tumor was excised and representative images were recorded. (C) Lewis cells were injected into C57BL/6 mice through tail vein to establish the tumor model of lung metastasis. Mice were treated as indicated and representative hematoxylin and eosin (H&E) images of mice lung nodules were shown in different groups ($n = 3$). (D) H&E and immunohistochemistry (IHC) staining of CD8, programmed cell death 1 ligand 1 (PD-L1), PD-1, granzyme B (GZMB) and Ki67 in mice subcutaneous tumor tissues of different groups. (E) Flow cytometry was used to analyze the proportion of $CD8^+$ $PD\text{-}1^+$ or $CD8^+$ $GZMB^+$ T cells in mice subcutaneous tumor tissues of different groups. The representative data of three independent experiments were shown.

most in the combination treatment group (Figs. 7D, 7E and S5E). And the proportion of exhausted T cells (PD-1 and CD8 double positive) presented an opposite trend, demonstrating that MAN remodels the tumor microenvironment.

4. Discussion

Mulberry leaves are traditional Chinese medicine, which are widely used to treat human respiratory diseases [34]. Previous studies have shown that methylene chloride extracts from mulberry leaves have anti-cancer and anti-inflammatory effect [35,36]. In our previous studies, several secondary metabolites have been successfully extracted from mulberry leaves [13,30,31], such as MAN, GSE, CMR etc. Pharmacological studies have also revealed that these secondary metabolites have a wide range of biological activities [13,37]. However, most studies only focused on one or two signaling pathways, making it impossible to fully understand the mechanism of action of these secondary metabolites. Comparative proteomic analysis has also been applied to identify the differential proteins in response to these secondary metabolites' treatment. Although it provides a comprehensive overview of cellular changes, it is hard to distinguish between primary and secondary effects [13,37].

In the current study, one secondary metabolite of mulberry leaves MAN was chosen and modified for in-depth analysis. This study provides a comprehensive review of the anti-cancer effect of secondary metabolite of mulberry leaves and serves as useful references for their future clinical application. In this case, we introduced a tiny alkynyl group into MAN to create an activity-based probe. Unlike bulky biotin labels, small alkynyl groups do not affect the ability of compounds to penetrate cellular plasma membrane, thus the probe of MAN can be used to target proteins in the body (Fig. 2C). MAN and its probe displayed similar inhibitory effect on lung cancer cell growth (Fig. 1D). In addition, non-specific binding proteins and endogenous biotinylated proteins are filtered by quantitative proteomics, which enhances the reliability of identified protein targets. Moreover, our method can also be applied to the study of MAN targets in normal cells parallel to cancer cells and combination with quantitative proteomics can further identify the most critical targets for the anti-cancer properties of MAN.

The immunomodulatory effects of mulberry leaf extract have been previously reported, which is able to boost immune response [16]. Our KEGG enrichment analysis of MAN targets showed that several immune-related pathways were involved (Fig. 3E), including PD-L1 checkpoint, TCR signaling, TNF-α signaling etc., indicating the immunoregulatory function of MAN. More importantly, several immune checkpoint molecules were directly bound by MAN (Fig. 3F), such as PD-L1, HLA etc. To confirm our findings, we used SPR to investigate the affinity between MAN and purified PD-L1 protein and found that MAN interacted with recombinant PD-L1 coated surface in a dose-dependent manner (Fig. 4A). Since we failed to obtain a crystal structure of complex, we could only attempt to understand the interaction at the molecular level by molecular docking. The key resides (Y32, K136, E158) of PD-L1 protein were predicted and validated for MAN binding (Fig. 4D), which locate in the extracellular domain of PD-L1 protein. Increasing evidence showed

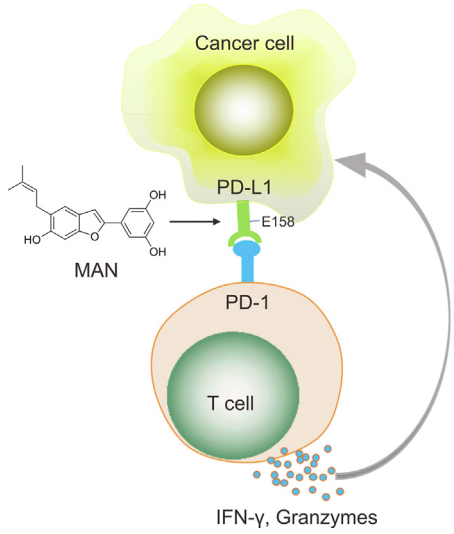

Fig. 8. The action mechanism of secondary metabolites of mulberry leaves in anti-lung cancer. Moracin N (MAN) and other products downregulated the expression of programmed cell death 1 ligand 1 (PD-L1) in lung cancer cells, disrupted the interaction of PD-L1/programmed cell death 1 (PD-1) and enhanced T cell-mediated immunity, ultimately suppressing the tumorigenesis of lung cancer. IFN-γ: interferon-γ.

that PD-L1 protein stability is regulated by multiple pathways [38]. PD-L1 undergoes ubiquitination and degradation by E3 ubiquitin ligases such as STUB1, Cullin3^{SPOP} and β-TrCP [2,39–41]. GSK3β interacts with PD-L1 and induces its phosphorylation at Y180/S184, resulting in β-TrCP ubiquitin ligase-mediated PD-L1 ubiquitination and degradation [42]. AMPK induces PD-L1 phosphorylation at S195, leading to abnormal PD-L1 glycosylation and ER-associated protein degradation [43]. Under MAN treatment, the expression levels of PD-L1 were downregulated, which may be attributed to the increased phosphorylation level of PD-L1 (Fig. 5I).

Cancer cells are able to disrupt T-cell-mediated immune surveillance through PD-L1 expression [44]. PD-L1 binds to PD-1 molecule of lymphocytes and inhibits their activation and weakens the anti-tumor immune response of the body [45]. In recent years, immune checkpoint inhibitors, including anti-PD-1 and anti-PD-L1 antibodies, have become new therapies for lung cancer [46]. However, their response rate remains limited with less than 20% [47]. Thus, small molecule inhibitors that can disrupt PD-L1-mediated tumor tolerance or improve immunotherapy efficacy are imperative to develop. Here, our preliminary results showed that mulberry leaves extract promoted the degradation and the immunosuppressive molecule PD-L1 and disrupted the PD-L1/PD-1 axis to enhance T-cell-mediated immunity (Figs. 5, 7 and S2). More importantly, MAN and anti-PD-1 antibody had achieved a synergistic anti-tumor effect through enhancing the function of cytotoxic T cells and decreasing the proportion of exhausted T cells (Fig. 8), either in primary or metastatic lung cancer. Because of their good safety, it has great potential to be applied in clinical practices. Traditional Chinese medicine is often used as an adjuvant therapy for different cancer [48]. Either Chinese medicine monomers or herbal formulas are a multi-target system of medicine known for enhancing anti-cancer immunity through modulating the tumor immune microenvironment [49]. But in clinical practices, Chinese herbal formula use is still limited due to the lack of clarity in their pharmacodynamic ingredients and accuracy of the compound's concentration. With the advancement of herb genomics research, a comprehensive Chinese medicine database will be built for clinical application and industrial development of Chinese medicine.

In conclusion, our results demonstrate that secondary metabolites of mulberry leaves target PD-L1 protein and inhibit the PD-L1/PD-1 signaling pathway in lung cancer, resulting in the activation of cytotoxic T cells and enhancement of anti-cancer immunity (Fig. 8). These findings reveal the molecular targets of mulberry leaves extract and emphasize the importance and great potential of secondary metabolites of mulberry leaves as traditional Chinese medicine in improving the efficacy of lung cancer immunotherapy.

5. Conclusions

These findings suggest that a novel anti-cancer mechanism of secondary metabolites of mulberry leaves and they can exert a synergistic anti-tumor effect to improve the efficacy of immunotherapy in lung cancer.

CRediT author statement

Guiqin Ye: Methodology, Validation, Formal analysis, Investigation, Data curation, Writing - Original draft preparation, Reviewing and Editing, Visualization; **Xin Sun**: Methodology, Data curation, Validation, Writing - Original draft preparation; **Jiuzhou Li**: Resources, Methodology, Writing - Editing and Reviewing; **Yuanyuan Mai**: Visualization, Software, Methodology; **Ruilan Gao**: Writing - Reviewing and Editing, Supervision; **Jianbin Zhang**: Funding acquisition, Investigation, Project administration.

Declaration of competing interest

The authors declare that there are no conflicts of interest.

Acknowledgments

This study was supported by the National Natural Science Foundation of China (Grant No.: 32070740), Zhejiang Provincial Natural Science Foundation (Grant No.: LZ23H160005), Natural Science Foundation of Jiangsu Province (Grant No.: BK20201197), and Zhejiang Provincial Outstanding Talent Project of Ten Thousand Talents Program, Zhejiang Provincial Qianjiang Talents Program to Jianbin Zhang.

Appendix A. Supplementary data

Supplementary data to this article can be found online at https://doi.org/10.1016/j.jpha.2023.12.016.

References

[1] S.C. Wei, C.R. Duffy, J.P. Allison, Fundamental mechanisms of immune checkpoint blockade therapy, Cancer Discov. 8 (2018) 1069–1086.
[2] C.W. Li, S.O. Lim, W. Xia, et al., Glycosylation and stabilization of programmed death ligand-1 suppresses T-cell activity, Nat. Commun. 7 (2016), 12632.
[3] M.E. Keir, M.J. Butte, G.J. Freeman, et al., PD-1 and its ligands in tolerance and immunity, Annu. Rev. Immunol. 26 (2008) 677–704.
[4] V.A. Boussiotis, Molecular and biochemical aspects of the PD-1 checkpoint pathway, N. Engl. J. Med. 375 (2016) 1767–1778.
[5] P. Sharma, J.P. Allison, Immune checkpoint targeting in cancer therapy: Toward combination strategies with curative potential, Cell 161 (2015) 205–214.
[6] C. Sun, R. Mezzadra, T.N. Schumacher, Regulation and function of the PD-L1 checkpoint, Immunity 48 (2018) 434–452.
[7] S.J. Park, H. Namkoong, J. Doh, et al., Negative role of inducible PD-1 on survival of activated dendritic cells, J. Leukoc. Biol. 95 (2014) 621–629.
[8] J. Sunshine, J.M. Taube, PD-1/PD-L1 inhibitors, Curr. Opin. Pharmacol. 23 (2015) 32–38.
[9] S.J. Bagley, J.M. Bauml, C.J. Langer, PD-1/PD-L1 immune checkpoint blockade in non-small cell lung cancer, Clin. Adv. Hematol. Oncol. 13 (2015) 676–683.
[10] L. Chen, X. Han, Anti-PD-1/PD-L1 therapy of human cancer: Past, present, and future, J. Clin. Invest. 125 (2015) 3384–3391.

[11] Y.M. Syah, S.A. Achmad, E.L. Ghisalberti, et al., Andalasin A, a new stilbene dimer from *Morus macroura*, Fitoterapia 71 (2000) 630–635.
[12] Y. Yang, Y. Tan, R. Chen, et al., The latest review on the polyphenols and their bioactivities of Chinese *Morus* plants, J. Asian Nat. Prod. Res. 16 (2014) 690–702.
[13] C. Gao, X. Sun, Z. Wu, et al., A novel benzofuran derivative moracin N induces autophagy and apoptosis through ROS generation in lung cancer, Front. Pharmacol. 11 (2020), 391.
[14] D.H. Kwon, J.M. Cheon, E.O. Choi, et al., The immunomodulatory activity of Mori folium, the leaf of *Morus alba* L., in RAW 264.7 macrophages *in vitro*, J. Cancer Prev. 21 (2016) 144–151.
[15] F. Aziz-Aliabadi, H. Noruzi, A. Hassanabadi, Effect of different levels of green tea (*Camellia sinensis*) and mulberry (*Morus alba*) leaves powder on performance, carcass characteristics, immune response and intestinal morphology of broiler chickens, Vet. Med. Sci. 9 (2023) 1281–1291.
[16] Y. Shan, C. Sun, J. Li, et al., Characterization of purified mulberry leaf glycoprotein and its immunoregulatory effect on cyclophosphamide-treated mice, Foods 11 (2022), 2034.
[17] G. Ma, X. Chai, G. Hou, et al., Phytochemistry, bioactivities and future prospects of mulberry leaves: A review, Food Chem. 372 (2022), 131335.
[18] T. Thaipitakwong, S. Numhom, P. Aramwit, Mulberry leaves and their potential effects against cardiometabolic risks: A review of chemical compositions, biological properties and clinical efficacy, Pharm. Biol. 56 (2018) 109–118.
[19] I.S. Parida, S. Takasu, K. Nakagawa, A comprehensive review on the production, pharmacokinetics and health benefits of mulberry leaf iminosugars: Main focus on 1-deoxynojirimycin, d-fagomine, and 2-O-α-d-galactopyranosyl-DNJ, Crit. Rev. Food Sci. Nutr. 63 (2023) 3468–3496.
[20] X. Chen, Y. Wang, N. Ma, et al., Target identification of natural medicine with chemical proteomics approach: Probe synthesis, target fishing and protein identification, Signal Transduct. Target. Ther. 5 (2020), 72.
[21] U. Rix, G. Superti-Furga, Target profiling of small molecules by chemical proteomics, Nat. Chem. Biol. 5 (2009) 616–624.
[22] E.J. van Rooden, B.I. Florea, H. Deng, et al., Mapping *in vivo* target interaction profiles of covalent inhibitors using chemical proteomics with label-free quantification, Nat. Protoc. 13 (2018) 752–767.
[23] D. Liu, C. Zou, J. Zhang, et al., Target profiling of an anticancer drug curcumin by an *in situ* chemical proteomics approach, Methods Mol. Biol. 2213 (2021) 147–161.
[24] L.A. Tang, J. Wang, T.K. Lim, et al., High-performance graphene-titania platform for detection of phosphopeptides in cancer cells, Anal. Chem. 84 (2012) 6693–6700.
[25] D. Pensold, G. Zimmer-Bensch, Methods for single-cell isolation and preparation, Adv. Exp. Med. Biol. 1255 (2020) 7–27.
[26] D.S. Goodsell, G.M. Morris, A.J. Olson, Automated docking of flexible ligands: Applications of AutoDock, J. Mol. Recognit. 9 (1996) 1–5.
[27] J. Qiu, B. Xu, D. Ye, et al., Cancer cells resistant to immune checkpoint blockade acquire interferon-associated epigenetic memory to sustain T cell dysfunction, Nat. Cancer 4 (2023) 43–61.
[28] X. Dai, X. Bu, Y. Gao, et al., Energy status dictates PD-L1 protein abundance and anti-tumor immunity to enable checkpoint blockade, Mol. Cell 81 (2021) 2317–2331.e6.
[29] H. Horita, A. Law, S. Hong, et al., Identifying regulatory posttranslational modifications of PD-L1: A focus on monoubiquitinaton, Neoplasia 19 (2017) 346–353.
[30] Y. Shu, H. Yuan, M. Xu, et al., A novel Diels-Alder adduct of mulberry leaves exerts anticancer effect through autophagy-mediated cell death, Acta Pharmacol. Sin. 42 (2021) 780–790.
[31] S. Zhang, X. Zhang, J. Liang, et al., Chalcomoracin inhibits cell proliferation and increases sensitivity to radiotherapy in human non-small cell lung cancer cells via inducing endoplasmic reticulum stress-mediated paraptosis, Acta Pharmacol. Sin. 41 (2020) 825–834.
[32] S. Lah, S. Kim, I. Kang, et al., Engineering second-generation TCR-T cells by site-specific integration of TRAF-binding motifs into the *CD247* locus, J. Immunother. Cancer 11 (2023), e005519.
[33] M. Reina-Campos, N.E. Scharping, A.W. Goldrath, $CD8^+$ T cell metabolism in infection and cancer, Nat. Rev. Immunol. 21 (2021) 718–738.
[34] S. Gupta, F. Afaq, H. Mukhtar, Selective growth-inhibitory, cell-cycle deregulatory and apoptotic response of apigenin in normal versus human prostate carcinoma cells, Biochem. Biophys. Res. Commun. 287 (2001) 914–920.
[35] S.H. Park, G.Y. Chi, H.S. Eom, et al., Role of autophagy in apoptosis induction by methylene chloride extracts of Mori cortex in NCI-H460 human lung carcinoma cells, Int. J. Oncol. 40 (2012) 1929–1940.
[36] T.R. Min, H.J. Park, M.N. Park, et al., The root bark of *Morus alba* L. suppressed the migration of human non-small-cell lung cancer cells through inhibition of Epithelial-Mesenchymal transition mediated by STAT3 and src, Int. J. Mol. Sci. 20 (2019), 2244.
[37] J. Tu, D. Shi, L. Wen, et al., Identification of moracin N in mulberry leaf and evaluation of antioxidant activity, Food Chem. Toxicol. 132 (2019), 110730.
[38] Q. Gou, C. Dong, H. Xu, et al., PD-L1 degradation pathway and immunotherapy for cancer, Cell Death Dis. 11 (2020), 955.
[39] R. Mezzadra, C. Sun, L.T. Jae, et al., Identification of CMTM6 and CMTM4 as PD-L1 protein regulators, Nature 549 (2017) 106–110.
[40] J. Zhang, X. Bu, H. Wang, et al., Cyclin D-CDK4 kinase destabilizes PD-L1 via cullin 3-SPOP to control cancer immune surveillance, Nature 553 (2018) 91–95.
[41] L. Deng, G. Qian, S. Zhang, et al., Inhibition of mTOR complex 1/p70 S6 kinase signaling elevates PD-L1 levels in human cancer cells through enhancing protein stabilization accompanied with enhanced β-TrCP degradation, Oncogene 38 (2019) 6270–6282.
[42] C. Xu, N.G. Kim, B.M. Gumbiner, Regulation of protein stability by GSK3 mediated phosphorylation, Cell Cycle 8 (2009) 4032–4039.
[43] J.H. Cha, W. Yang, W. Xia, et al., Metformin promotes antitumor immunity via endoplasmic-reticulum-associated degradation of PD-L1, Mol. Cell 71 (2018) 606–620.e7.
[44] P. Sharma, J.P. Allison, The future of immune checkpoint therapy, Science 348 (2015) 56–61.
[45] J.X. Caushi, J. Zhang, Z. Ji, et al., Transcriptional programs of neoantigen-specific TIL in anti-PD-1-treated lung cancers, Nature 596 (2021) 126–132.
[46] A. Lahiri, A. Maji, P.D. Potdar, et al., Lung cancer immunotherapy: Progress, pitfalls, and promises, Mol. Cancer 22 (2023), 40.
[47] M. Wang, L. Zhu, X. Yang, et al., Targeting immune cell types of tumor microenvironment to overcome resistance to PD-1/PD-L1 blockade in lung cancer, Front. Pharmacol. 14 (2023), 1132158.
[48] Y. Zhang, Y. Liang, C. He, Anticancer activities and mechanisms of heat-clearing and detoxicating traditional Chinese herbal medicine, Chin. Med. 12 (2017), 20.
[49] A.G. Atanasov, S.B. Zotchev, V.M. Dirsch, et al., Natural products in drug discovery: Advances and opportunities, Nat. Rev. Drug Discov. 20 (2021) 200–216.